THE JOURNAL OF PHYSICAL CHEMISTRY A

Article

pubs.acs.org/JPCA

Structural and Thermochemical Chemisorption of CO_2 on $Li_{4+x}(Si_{1-x}Al_x)O_4$ and $Li_{4-x}(Si_{1-x}V_x)O_4$ Solid Solutions

José Ortiz-Landeros,[†,‡] Carlos Gómez-Yáñez,[‡] Luis M. Palacios-Romero,[†] Enrique Lima,[†] and Heriberto Pfeiffer*[,†]

[†]Instituto de Investigaciones en Materiales, Universidad Nacional Autónoma de México, Circuito exterior s/n, Ciudad Universitaria, Del. Coyoacán, CP 04510, México DF, Mexico

[‡]Departamento de Ingeniería Metalúrgica, Escuela Superior de Ingeniería Química e Industrias Extractivas, IPN, UPALM, Av. Instituto Politécnico Nacional s/n, CP 07738, México DF, Mexico

ABSTRACT: Different Li_4SiO_4 solid solutions containing aluminum ($Li_{4+x}(Si_{1-x}Al_x)O_4$) or vanadium ($Li_{4-x}(Si_{1-x}V_x)O_4$) were prepared by solid state reactions. Samples were characterized by X-ray diffraction and solid state nuclear magnetic resonance. Then, samples were tested as CO_2 captors. Characterization results show that both, aluminum and vanadium ions, occupy silicon sites into the Li_4SiO_4 lattice. Thus, the dissolution of aluminum is compensated by Li^{1+} interstitials, while the dissolution of vanadium leads to lithium vacancies formation. Finally, the CO_2 capture evaluation shows that the aluminum presence into the Li_4SiO_4 structure highly improves the CO_2 chemisorption, and on the contrary, vanadium addition inhibits it. The differences observed between the CO_2 chemisorption processes are mainly correlated to the different lithium secondary phases produced in each case and their corresponding diffusion properties.

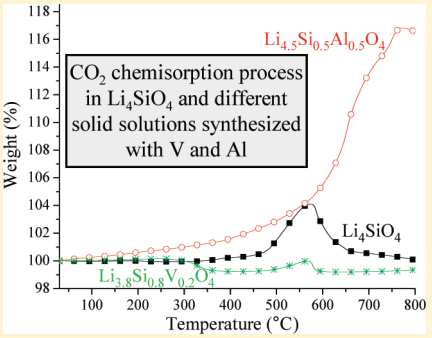

1. INTRODUCTION

The main drawback of the use of fossil fuels is the emission of carbon dioxide (CO_2) to the atmosphere that contributes to the greenhouse effect and the Earth global warming.[1] Thus, CO_2 has to be retained through either physical or chemical processes.[2−4] In the last years, several authors have reported the possible application of different lithium ceramics as CO_2 absorbents described as well as CO_2 captors.[5−27] These works have shown that lithium ceramics are able to retain CO_2.

Different authors have proved that during the CO_2 capture on lithium ceramics, the diffusion processes are the limiting step of the whole reaction.[6,16,23,28−30] Hence, several studies have been performed in order to elucidate the absorption mechanism as well as possible microstructural, structural, and/or chemical modifications of these lithium ceramic absorbents, seeking to enhance efficiency in the absorption and increments in CO_2 absorption rates. Few papers have proposed the synthesis of different solid solutions of lithium ceramics, which seem to show better CO_2 capture properties than those observed by the pure lithium ceramics. The solid solutions reported as possible CO_2 captors are $Li_{2-x}Na_xZrO_3$, $Li_{3.7}Al_{0.1}SiO_4$, $Li_{3.7}Fe_{0.1}SiO_4$, and $Li_{4-x}Na_xSiO_4$.[6−8,10,11,31] In general, all these solid solutions seem to improve different properties of the CO_2 absorption reaction, in comparison to their respective pure alkaline ceramics. The improvements observed on the different solid solutions have been attributed to the formation of point defects in the lattice or the formation of secondary phases, which seem to improve diffusion processes, the limiting step of the CO_2 capture process.

However, the conductivity properties of this kind of ceramics and different solid solutions have been widely studied for the design and production of ionic conductors.[32,33] This information may be used on the design of new CO_2 captor lithium ceramics since the ion conduction is totally correlated to the diffusion process.[34] Among the lithium ceramics, different ionic conduction studies have been performed on the Li_4SiO_4,[32,33,35−37] an excellent CO_2 captor.[5,6,10,13−15,30] These reports include the solid solution syntheses of Li_4SiO_4 with different di- and trivalent cations (B^{3+}, Al^{3+}, Ga^{3+}, Cr^{3+}, Fe^{3+}, Ni^{2+}, and Co^{2+}) or even pentavalent cations (P^{5+}, As^{5+}, and V^{+5}). For example, it has been proved that in both cases Al^{3+} or V^{5+}substitution on the Li_4SiO_4 structure enhances the lithium ion conduction of these materials.[37−40]

In the same sense, some thermodynamic considerations on the same ceramics and their solid solutions have been proposed. Thangadurai and Weppner[41] proposed the Li_4SiO_4 solid solution synthesis with different metal oxides having more negative Gibbs free energy of formation (ΔG_f) than that of SiO_2. The elements reported were M = B, Al, Ga, and Cr. In all these cases, when the M−O bond attraction was increased, the Li−O interaction decreased and consequently the lithium ion conductivity was improved.

Summarizing, different Li_4SiO_4 solid solutions should present desirable behaviors as CO_2 absorbents, if the element substituting the silicon atoms presents some of the character-

Received: January 18, 2012
Revised: March 6, 2012
Published: March 6, 2012

istics described above. Then, the aim of this work was to synthesize, characterize, and determine systematically the CO_2 absorption process of the following lithium orthosilicate solid solutions: $Li_{4+x}(Si_{1-x}Al_x)O_4$ and $Li_{4-x}(Si_{1-x}V_x)O_4$. Aluminum and vanadium were chosen as silicon substituting elements since they possess different atomic charges than Si^{4+}; aluminum has a smaller charge (3+), while vanadium has a larger charge (5+). Therefore, the lithium ion conductivity can be promoted by the formation of point defects as a result of charge compensation. Additionally, the ΔG_f of the metal oxide of both elements are more negative than that of SiO_2 (−856.3 kJ/mol). The aluminum and vanadium oxides have the following ΔG_f values: −1582.3 and −1419.5 kJ/mol, respectively.[42] Finally, it has to be mentioned that previous papers have shown that aluminum may be located at two different positions into the Li_4SiO_4 structure, either at the silicon or lithium atomic positions.[10]

2. EXPERIMENTAL SECTION

Two different solid solution series $(Li_{4+x}(Si_{1-x}Al_x)O_4$ and $Li_{4-x}(Si_{1-x}V_x)O_4)$ were prepared by solid-state reactions. In the first case, $Li_{4+x}(Si_{1-x}Al_x)O_4$ solid solutions were synthesized by a solid-state reaction performed between Li_4SiO_4 and Li_5AlO_4, where the two precursors were synthesized by solid state reaction as well. Li_4SiO_4 was obtained by mixing, in water, lithium hydroxide (LiOH, Aldrich) and fumed silica (SiO_2, Sigma-Aldrich), with a Li/Si molar ratio of 4.1:1. After a few hours, the suspension was heated at 70 °C, and the final powder was calcined at 700 °C for 4 h. At the same time, Li_5AlO_4 was synthesized mixing in an Agatha mortar α-alumina (α-Al_2O_3, Aldrich) and lithium oxide (Li_2O, Aldrich), with a Li/Al molar ratio of 5.5:1. Then, powders were calcined at 900 °C for 44 h. The production of Li_4SiO_4 and Li_5AlO_4 phases was verified by XRD (data not shown). After that, the $Li_{4+x}(Si_{1-x}Al_x)O_4$ solid solutions were prepared by mixing mechanically the corresponding amounts of Li_4SiO_4 and Li_5AlO_4, where $0.05 \leq x \leq 0.5$. Powders were pelletized (5 ton/cm^2) and calcined at 850 °C for 12.5 h. Finally, the pellets were pulverized in an Agatha mortar. In the case of the $Li_{4-x}(Si_{1-x}V_x)O_4$ solid solution syntheses ($0.05 \leq x \leq 0.2$), the precursors used were Li_4SiO_4, vanadium pentoxide (V_2O_5, Aldrich), and Li_2O. As in the previous case, these compounds were mechanically mixed, pressed, and calcined at the same conditions.

Samples were labeled according to the substitutional element (Al or V) and the corresponding x value, for example, the V20 sample corresponds to the vanadium solid solution with the following nominal composition $Li_{3.8}(Si_{0.8}V_{0.2})O_4$. The initial Li_4SiO_4 was equally analyzed for comparison purposes, and it was simply called Li_4SiO_4.

All the solid solutions were characterized by powder X-ray diffraction (XRD) and multinuclear solid-state nuclear magnetic resonance (MAS NMR). The XRD patterns were obtained with a D8 Bruker diffractometer coupled to a Cu anode X-ray tube in Bragg−Brentano configuration. The $K_{\alpha 1}$ wavelength was selected with a diffracted beam Ge monochromator, and the compounds were identified conventionally using the Joint Compounds Powder Diffraction Standards (JCPDS) database. The experimental error was ±3%. Rietveld structural refinements were performed using the FullProf-Suite software.[43] The background was approximated by a polynomial function of θ. The profile function, which was used to describe the peak shape, was a Thompson−Cox−Hastings pseudo-Voigt function. The instrumental profile was determined by the Caglioti function,[44] where the parameters u, v, and w were refined for the LaB_6 standard in order to be incorporated in the solid solution refinements.

NMR spectra were acquired on a Bruker Avance II spectrometer with a magnetic field strength of 7.05 T, corresponding to a ^{27}Al Larmor frequency of 78.3 MHz. Short single pulses ($\pi/12$) with a recycle time of 0.5 s were used. Samples were packed into zirconia rotors 4 mm o.d. The ^{27}Al chemical shift was expressed as ppm from an aqueous solution of $Al(NO_3)_3$ as external standard. ^{29}Si MAS NMR spectra were obtained operating the spectrometer at a resonance frequency of 59.59 MHz with a recycling time of 40 s and a pulse time of 3 μs. The spinning frequency was 5 kHz, and tetramethylsilane (TMS) was used as a reference. ^{51}V MAS NMR spectra were acquired at 78.89 MHz. Single $\pi/2$ pulses were used. Samples were spun at 5 kHz, and $VClO_3$ was used to reference the chemical shifts. Finally, ^{6}Li and ^{7}Li NMR measurements were carried out at resonance frequencies of 44.14 and 116.57 MHz, respectively. The chemical shifts are relative to an external powder sample of LiCl set at 0 ppm.

Thermogravimetric analyses (TGA) were performed with a Q500HR equipment from TA Instruments. The solid solutions were heat treated with a heating rate of 5 °C min^{-1} from room temperature to 800 °C. These analyses were carried out under a saturated CO_2 atmosphere, using a CO_2 flow of 60 mL/min. Finally, it must be pointed out that solid solutions did not present any important microstructural differences among them (data not shown), which might alter the CO_2 chemisorption results.

3. RESULTS AND DISCUSSION

Al^{3+} and V^{5+} were chosen as substitutional elements, on the Li_4SiO_4 structure, due to different chemical considerations such as crystalline structure, coordination, and electronegativity, as well as due to the chemistry of defects and some thermodynamic factors related to the formation Gibbs free energy (ΔG_f), which have been already mentioned in the introduction section. Figure 1 shows the XRD patterns of the different solid solutions, $Li_{4+x}(Si_{1-x}Al_x)O_4$ and $Li_{4-x}(Si_{1-x}V_x)O_4$ as well as the Li_4SiO_4 sample. As it can be seen, all the $Li_{4+x}(Si_{1-x}Al_x)O_4$ solid solutions were fitted to the Li_4SiO_4 diffraction pattern (JCPDS file 76−1085). In this case, the x value was not further increased as it implies the lithium decrement into the structure. However, the $Li_{4+x}(Si_{1-x}Al_x)O_4$ solid solutions showed a complete aluminum dissolution up to $x \leq 0.5$. However, it has to be mentioned that the $Li_{4+x}(Si_{1-x}Al_x)O_4$ samples with $x \geq 0.3$ had to be mixed and calcined twice in order to obtain a complete aluminum solubility. Otherwise, a secondary phase was detected, Li_5AlO_4 (JCPDS file 70−0432). As it could be expected, XRD patterns showed some profile changes as a function of the Al or V addition (Figure 2). In both cases, the XRD patterns showed a left shift, which qualitatively indicates that the crystalline structure has been expanded. It can be explained by the fact that V^{5+} (0.036 nm) and Al^{3+} (0.039 nm) possess larger ionic radii than Si^{4+} (0.026 nm). Additionally, in the Al^{3+} case, there must be a smaller electronic attraction than that of Si^{4+}, which contributes to the cell expansion. On the contrary, although V^{5+} must produce a stronger attraction, its larger ionic radius must finally produce the cell expansion. Moreover, it has to be taken into account the fact that vanadium addition

dx.doi.org/10.1021/jp3006298 | J. Phys. Chem. A 2012, 116, 3163−3171

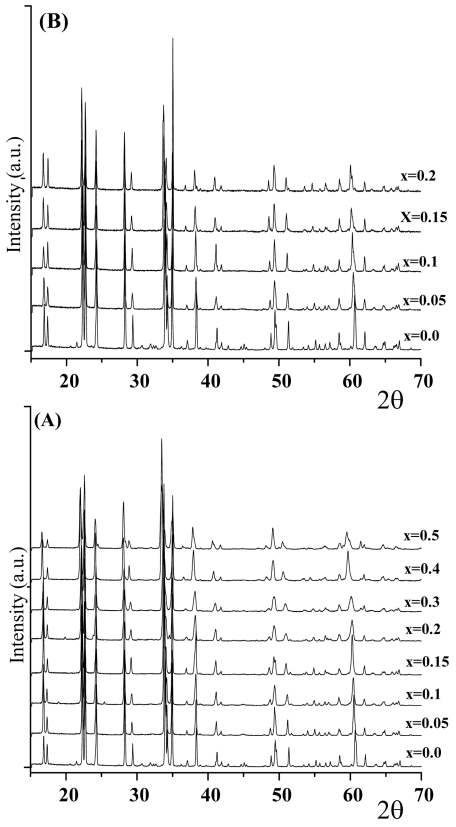

Figure 1. XRD patterns of the (A) $Li_{4+x}(Si_{1-x}Al_x)O_4$ and (B) $Li_{4-x}(Si_{1-x}V_x)O_4$ solid solutions. The corresponding x values are presented in the figures, where x = 0.0 corresponds to Li_4SiO_4.

produces lithium vacancies, which contribute, as well, to these cell changes.

In order to verify the XRD results observed above, a Rietveld refinement analysis was performed on both series of solid solutions, assuming that Al^{3+} or V^{5+} occupied Si^{4+} structural positions, although during simulation these solute ions were not taken into account. Additionally, it has to be mentioned that this analysis was only performed on the solid solutions with x values between 0 and 0.2, for comparison purposes. All the samples fitted reasonably to the Rietveld analyses. The cell parameters and the R_{wp} values obtained in each case are presented on the Table 1. Initially, it can be mentioned that R_{wp} values show that the refinements can be considered as acceptable, assuming the Al and V incorporation into the Li_4SiO_4 structure. In both cases, $Li_{4+x}(Si_{1-x}Al_x)O_4$ and $Li_{4-x}(Si_{1-x}V_x)O_4$, the cell parameter b and c, as well as the cell volume, tended to increase as a function of the Al or V content. However, the cell parameters values, a and β, did not show significant changes. Finally, it must be mentioned that the lithium occupancy coefficient in Li_4SiO_4 (6.592, considering two Li_4SiO_4 formulas per cell) varied depending on the substitution element. While the lithium occupancy decreased with the vanadium addition, the lithium occupancy increased with the aluminum addition in the concentration ranges studied here. However, it has to be taken into account that the formation of $Li_{4+x}(Si_{1-x}Al_x)O_4$ solid solutions implies the incorporation of lithium in excess; additionally, it must be considered that the Rietveld analysis is not very accurate for lithium since it is a very light atom.[11] Therefore, only the lithium occupancy tendencies should be taken into consideration. In other words, lithium occupancy decreased as a function of the vanadium addition, while lithium occupancy increased with the aluminum content, as it could be expected.

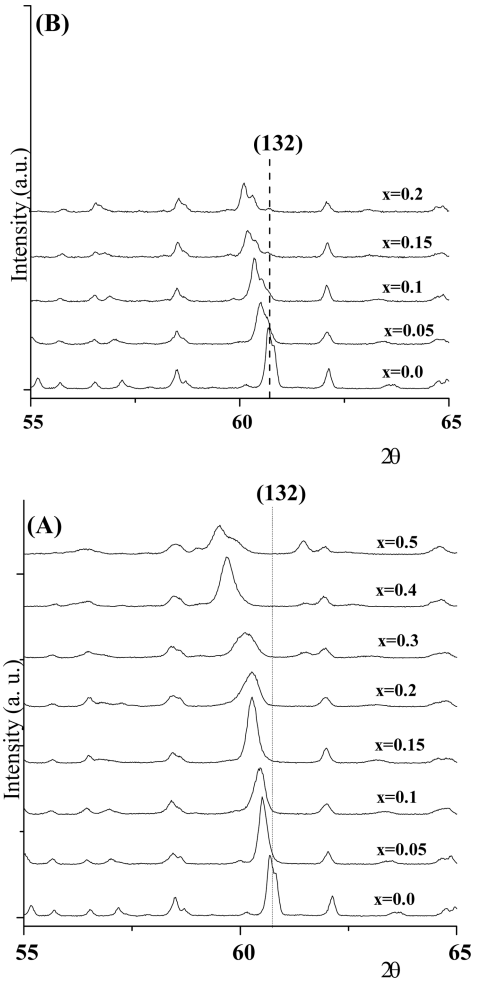

Figure 2. Zoom of the XRD patterns of the (A) $Li_{4+x}(Si_{1-x}Al_x)O_4$ and (B) $Li_{4-x}(Si_{1-x}V_x)O_4$ solid solutions. The corresponding x values are presented in the figures, where x = 0.0 corresponds to Li_4SiO_4.

Table 1. Rietveld Refinement Data Obtained from the Different $Li_{4+x}(Si_{1-x}Al_x)O_4$ and $Li_{4-x}(Si_{1-x}V_x)O_4$ Solid Solutions

	cell parameters (Å)					
sample	a	b	c	β (deg)	cell volume $(Å)^3$	R_{wp}
ref	5.147	6.094	5.293	90.33	166.02	
Li_4SiO_4	5.150	6.100	5.297	90.33	166.44	14.34
V5	5.152	6.117	5.314	90.27	167.52	11.86
V10	5.147	6.125	5.3261	90.26	167.93	10.16
V15	5.144	6.140	5.338	90.23	168.62	8.13
V20	5.141	6.149	5.347	90.25	169.07	9.47
Al5	5.154	6.120	5.311	90.27	167.55	14.76
Al10	5.155	6.127	5.315	90.28	167.90	11.54
Al15	5.155	6.156	5.327	90.32	169.08	11.47
Al20	5.154	6.159	5.328	90.27	169.14	13.84

In order to corroborate the XRD results and to further analyze both solid solutions, different solid-state NMR analyses were performed. ^{29}Si, ^{7}Li, ^{6}Li, and ^{27}Al or ^{51}V MAS NMR spectra were acquired to completely understand the solid

dx.doi.org/10.1021/jp3006298 | J. Phys. Chem. A 2012, 116, 3163−3171

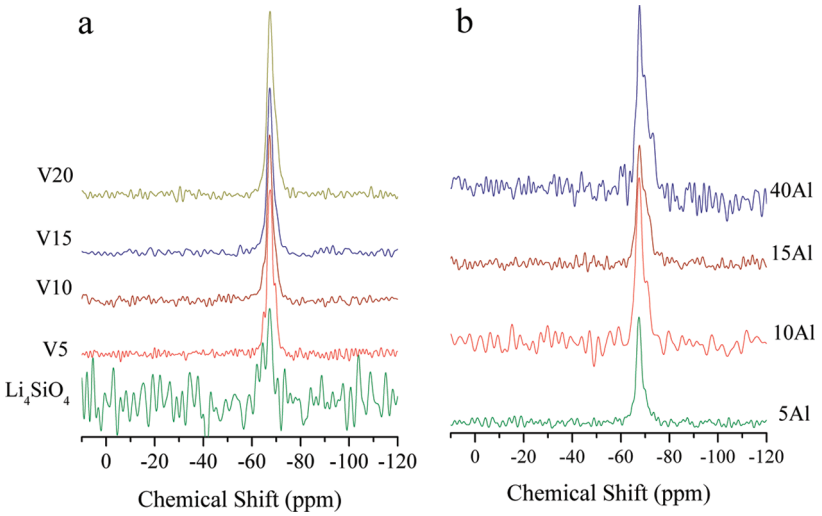

Figure 3. ^{29}Si MAS NMR of the $Li_{4-x}(Si_{1-x}V_x)O_4$ (a) and $Li_{4+x}(Si_{1-x}Al_x)O_4$ (b) solid solutions. The NMR spectrum corresponding to the Li_4SiO_4 was included for comparison purposes.

solution structures. Initially, the ^{29}Si MAS NMR spectra of both solid solutions are presented in Figure 3. In the $Li_{4-x}(Si_{1-x}V_x)O_4$ series, Figure 3a, only singlet ^{29}Si NMR peaks were observed even when a high percentage of silicon was replaced by vanadium. The peak observed at −67 ppm appears in the spectra of the vanadium containing samples as well as in the spectrum of the Li_4SiO_4 sample. This peak is assigned to Q_0 units present in the −Si−O−Si−O−Si− network. From ^{29}Si NMR results, it seems that vanadium did not modify the neighborhood of $[SiO_4]^{4-}$ tetrahedral, but, it should be emphasized that silicon nuclei have a spin of 1/2, and second order effects are absent because there are not quadrupole interactions. The spectra $Li_{4+x}(Si_{1-x}Al_x)O_4$ series (Figure 3b) evolves more interestingly; at very low aluminum content (sample 5Al) only the single peak at −67 ppm was observed. However, if aluminum content was increased, the initial peak turns to be decomposed by two other overlapped peaks, which appeared at stronger fields (−69 and −72 ppm). Additionally, the intensity of these two resonances increased with the aluminum content. These two resonances cannot be assigned to the formation of $[SiO_4]^{4-}$ surrounded by aluminum atoms as second neighboring from silicon nuclei because the resonances of these species are expected at weaker fields (chemical shifts lower than −80 ppm). Then, it should be attributed to the formation of $[SiO_4]^{4-}$ relatively isolated that could be the consequence of Si−O−Si angle modifications. These results are in good agreement with a previous paper, showing that aluminum addition into the silicon atomic positions produces this effect, while the addition of aluminum at the lithium sites generates a totally different NMR spectra.[45]

In this sense, Figure 4 displays the corresponding ^{27}Al MAS NMR spectra. It can be observed that there are two overlapped resonance peaks at 82 and 68 ppm, which mean that the lattice contains two types of aluminum 4-fold coordinated. At low aluminum concentrations, the relative intensity of these two resonances is, roughly, the same, but an augment in the aluminum percentage enhances the intensity of the resonance at 68 ppm, which has to be understood as a shielding of the aluminum nuclei. This can be due to a distortion of the aluminum sites with, possibly, a shortness of the Al−O distances. Another remark must be mentioned: the resonance peaks become broader with the aluminum content, which can

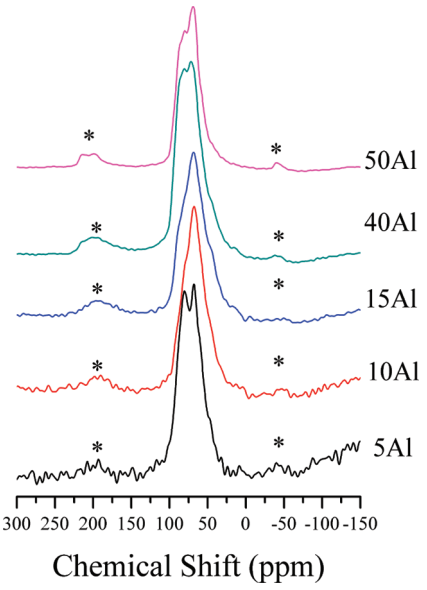

Figure 4. ^{27}Al MAS NMR of the $Li_{4+x}(Si_{1-x}Al_x)O_4$ solid solutions.

be due to that, at high aluminum loading, the probability to find an aluminum atom near another aluminum atom increases. Thus, quadrupolar interactions take place. Again, the presence of two well-defined overlapped peaks is in good agreement with the previous NMR study performed on Li_4SiO_4-based solid solutions containing aluminum at the silicon sites.[45]

Now, coming back to the $Li_{4-x}(Si_{1-x}V_x)O_4$ series. In the ^{51}V NMR spectra (Figure 5), independently of the vanadium content, only a single NMR peak was observed with constant line broadening effects arising from second order quadrupolar and chemical shift anisotropic interactions. The isotropic peak was observed from −562 to −572 ppm. The position of the peak goes to higher chemical shifts when vanadium content increased. This result suggests two features: first, the presence of tetrahedrally coordinated vanadium ions, which are replacing partially the silicon ions, and second, the higher the vanadium content, the lower the vanadium shielding. This can be explained because of the formation of microdomains enriched in V−O−V species. This result implies that oxygen charge is

dx.doi.org/10.1021/jp3006298 | J. Phys. Chem. A 2012, 116, 3163−3171

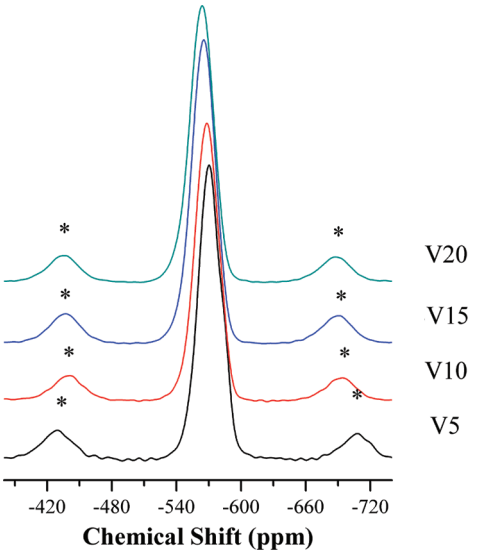

Figure 5. ^{51}V MAS NMR of the $Li_{4-x}(Si_{1-x}V_x)O_4$ solid solutions.

distributed for two highly positively charged atoms (V^{5+}), instead two Si^{4+} ions as occurs in the vanadium-free sample. It should be noticed that the absence of a signal close to −300 ppm supports that V_2O_5 phase is not present.

The ^{7}Li MAS NMR spectra for the $Li_{4-x}(Si_{1-x}V_x)O_4$ samples are displayed in Figure 6a. Only one ^{7}Li isotropic signal was observed at 1 ppm meaning that ^{7}Li NMR senses only one lithium site in the Li_4SiO_4 phase. The absence of signal close to 3 ppm indicates that Li^+ ions are not recombined with O^{2-} to form Li_2O. The ^{7}Li spinning sideband (SSB) intensities were very similar in all spectra suggesting a high anisotropy in all samples, even in the noncontaining vanadium sample. The only significant difference was the line width of the resonances. The higher the vanadium content, the broader the resonance line. ^{7}Li is a quadrupolar nucleus (spin 3/2); its resonance is strongly altered by quadrupolar and dipolar interactions, which enhances the broadening of the NMR peaks. Note that vanadium addition would increase the entropy of the material, in such a way that the electric field gradient changed. It seems that the interactions between lithium and oxygen−vanadium species modify the Li−O and Li−Li distances, altering then the spin diffusion process. However, the aluminum presence on the Li_4SiO_4 lattice induces the same broadening resonance line effect as observed in the spectra of $Li_{4+x}(Si_{1-x}Al_x)O_4$ samples, Figure 6b.

The other NMR active isotope of lithium is ^{6}Li, which possess a quadrupole moment 50 times smaller than that for ^{7}Li.[46] Thus, the ^{6}Li MAS NMR spectra shown in Figure 7a,b have mainly the contribution of the chemical shift interactions. Actually, ^{6}Li MAS NMR spectrum of the Li_4SiO_4 sample, Figure 7a, presents the peaks due to Li 3-fold, 4-fold, 5-fold, and 6-fold coordinated in an oxygen environment at 2.1, 0.6, −0.2, and −0.9 ppm, respectively.[47] With the incorporation of vanadium into the silicate lattice, the resonances due to lithium 3-fold (Li^{III}) and 5-fold (Li^{V}) coordinated practically disappeared for vanadium concentrations as low as 10% (sample V10). However, the 6-fold (Li^{VI}) coordinated lithium species persist even in the sample V15, but in the sample with the highest content of vanadium, sample V20, only the 4-fold coordinated lithium species were observed. The trend in the ^{6}Li MAS NMR spectra of $Li_{4+x}(Si_{1-x}Al_x)O_4$, Figure 7b, was different than that observed in the vanadium containing samples. It is not clear why when the aluminum content increased, the resonances due to species Li^{III}, Li^{V}, and Li^{VI} faded out. Actually, it should be emphasized that on the aluminum samples, ^{6}Li resonances become broader and the NMR peak of the sample Al50 is composed by a single width resonance peak due to Li^{IV}. As mentioned above, ^{6}Li nuclei has a very low quadrupole moment, so the chemical shift interactions dominate the spectrum. Hence, the peak broadness could be due to a decreasing of the motion of lithium atoms, which is consistent with Li^{1+} in interstitials sites.

After the whole structural analysis performed by XRD and NMR, it was proved that Al and V atoms are incorporated into the Li_4SiO_4 lattice at the Si sites, producing the respective $Li_{4+x}(Si_{1-x}Al_x)O_4$ and $Li_{4-x}(Si_{1-x}V_x)O_4$ solid solutions. The compensation defects produced by the solid solution formation can be written, using the Kröger−Vink notation, as follows:

$$Li_4SiO_4 + Li_5AlO_4 \xrightarrow{Li_4SiO_4} 8Li_{Li} + Si_{Si} + Al'_{Si} + Li_i^{\bullet} + 8O_O \quad (1)$$

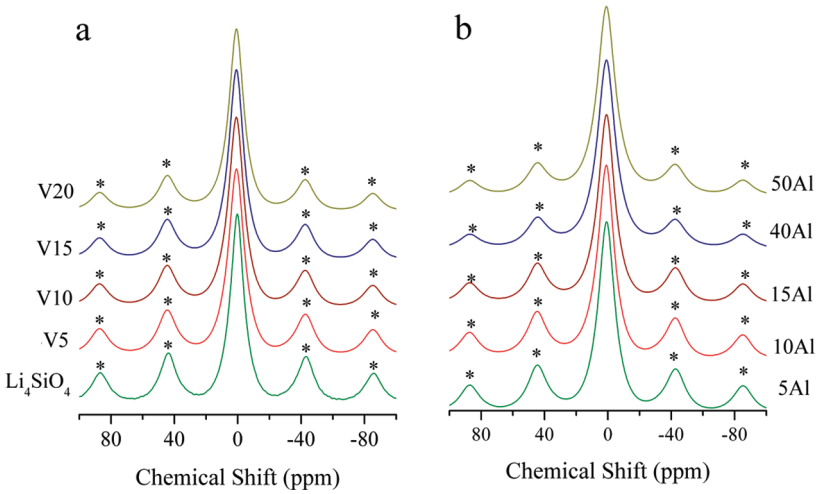

Figure 6. ^{7}Li MAS NMR of the $Li_{4-x}(Si_{1-x}V_x)O_4$ (a) and $Li_{4+x}(Si_{1-x}Al_x)O_4$ (b) solid solutions.

dx.doi.org/10.1021/jp3006298 | J. Phys. Chem. A 2012, 116, 3163−3171

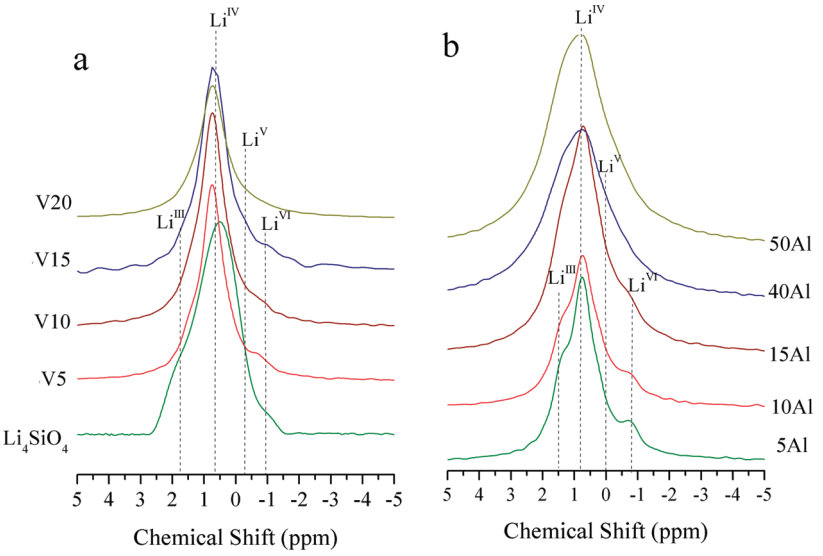

Figure 7. ^{6}Li MAS NMR spectra. Free and containing vanadium samples (a) and samples containing aluminum (b).

$$Li_4SiO_4 + 1.5Li_2O + 0.5V_2O_5 \xrightarrow{Li_4SiO_4} 7Li_{Li} + Si_{Si} + V_{Si}^{\bullet} + Va_{Li}' + 8O_O \quad (2)$$

As it can be seen, these two structures present some interesting differences. While the aluminum addition produces the presence of Li^{1+} interstitial atoms, the vanadium presence implies the lithium vacancies formation. Both, lithium interstitial atoms and lithium vacancies increase in proportion of the aluminum and vanadium addition into the Li_4SiO_4 solid solutions. In the aluminum case, the lithium diffusion is expected to be improved due to the lithium interstitial atoms, which implies a lithium excess, in comparison to the Li_4SiO_4 structure. Also, the structural changes produced by the aluminum atoms could help. Conversely, in the vanadium case, lithium diffusion would be improved due to the presence of vacancies, although it has to be taken into consideration the fact that, in this case, the lithium content decreased as a function of the vanadium addition. Therefore, these structural and composition modifications may change the CO_2 capture in two different aspects: (1) the CO_2 chemisorption reaction rate may be modified due to the different structural defects produced in each case, and (2) the external shell composition is going to change, varying the diffusion processes through it.

Additionally, as the lithium content and molecular weight varied as a function of the aluminum and vanadium addition, the CO_2 theoretical chemisorption varied, as it is shown in Table 2. The aluminum addition increases the CO_2 chemisorption capacity, as these solid solutions have more lithium atoms than Li_4SiO_4, and the molecular weights did not vary significantly. The silicon and aluminum weights only vary in ~1 g/mol. Conversely, the vanadium solid solutions decreased their CO_2 chemisorption capacity, as they contain less lithium, but mainly because vanadium is considerably heavier than silicon.

Thus, in order to analyze the influence of these structural modifications on the CO_2 capture properties of Li_4SiO_4, different experiments were performed. Figures 8 and 9 present the $Li_{4+x}(Si_{1-x}Al_x)O_4$ and $Li_{4-x}(Si_{1-x}V_x)O_4$ dynamic thermograms into a CO_2 flux. In both figures, the Li_4SiO_4 system is included for comparison purposes. In the case of the vanadium samples (Figure 8), it is evident that CO_2 capture decreases as a function of the vanadium content. Initially, between 280 and 360 °C samples lost ~1 wt %, attributed to a dehydroxylation process. It should be mentioned that the hydroxylation process

Table 2. Molecular Weights and CO_2 Theoretical Chemisorption Capacity of the $Li_{4-x}(Si_{1-x}V_x)O_4$ and $Li_{4+x}(Si_{1-x}Al_x)O_4$ Solid Solutions

		CO_2 chemisorption capacity	
sample	molecular weight (g/mol)	wt %	mmol/g
Li_4SiO_4	120.0	36.6	8.3
V5	120.8	35.5	8.1
V10	121.6	34.4	7.8
V15	122.4	33.2	7.6
V20	123.2	32.1	7.3
Al5	120.3	37.5	8.5
Al10	120.6	38.3	8.7
Al20	121.2	39.9	9.1
Al30	121.8	41.5	9.4
Al40	122.4	43.1	9.8
Al50	123.0	44.7	10.2

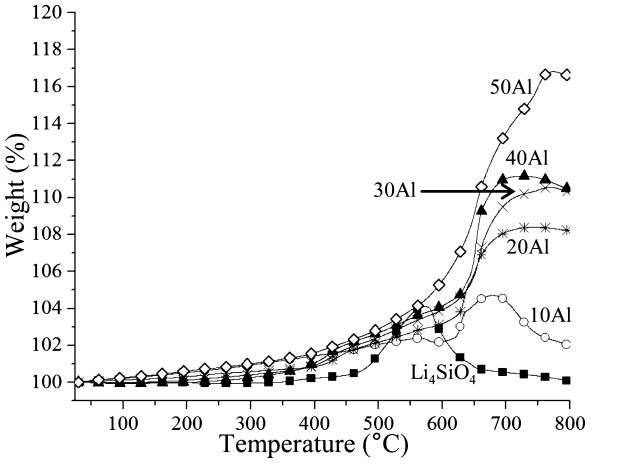

Figure 8. Thermogravimetric dynamic analyses of different $Li_{4+x}(Si_{1-x}Al_x)O_4$ solid solutions in a flux of CO_2.

dx.doi.org/10.1021/jp3006298 | J. Phys. Chem. A 2012, 116, 3163−3171

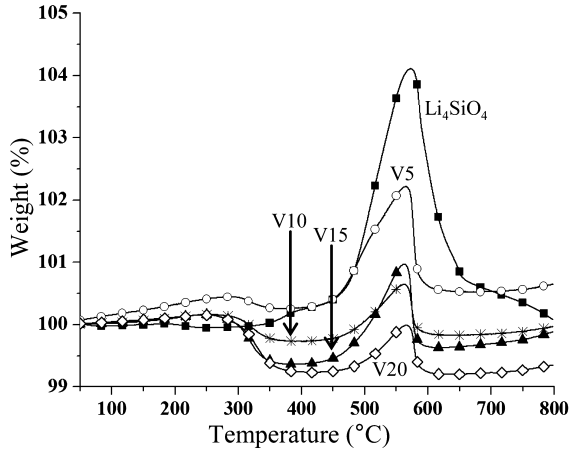

Figure 9. Thermogravimetric dynamic analyses of different $Li_{4-x}(Si_{1-x}V_x)O_4$ solid solutions in a flux of CO_2.

seems to be favored with the vanadium content. After that, the samples began to chemisorb CO_2 at approximately 450 °C. All the vanadium samples chemisorbed CO_2 in the same temperature range. Li_4SiO_4 chemisorbed the highest CO_2 quantity, 4.1 wt %. After that, CO_2 chemisorption decreased as a function of the vanadium content from 2.3 to 0.8 wt % on the V5 and V20 samples, respectively. Although these dynamic thermograms are qualitative, the curves in Figure 8 suggest that the CO_2 chemisorption kinetic process is hindered by the vanadium addition. While the Li_4SiO_4 sample presented a slope equal to 0.037 wt %/°C, the corresponding slope of the V20 sample decreased up to 0.008 wt %/°C.

It has to be emphasized that aluminum addition improved the CO_2 chemisorption on Li_4SiO_4, but the chemisorption temperature range was shifted to higher temperatures (Figure 9). All the aluminum samples began to chemisorb CO_2 at lower temperatures than that observed on the Li_4SiO_4 sample (450 °C). In fact, these samples chemisorbed up to 1 wt % between room temperature and 370 °C. This behavior is in good agreement with a previous report showing the CO_2 capture on two different samples; $Li_{4.1}Al_{0.1}Si_{0.9}O_4$ and $Li_{3.7}Al_{0.1}SiO_4$.[10] After that, all the aluminum containing samples presented a second well-defined CO_2 capture between 380 and 570 °C. Finally, samples presented the highest CO_2 chemisorption between 600 and 770 °C. In fact, the last CO_2 capture process has a very similar trend than that observed on Li_5AlO_4.[16] Furthermore, it must be mentioned that the aluminum content increased the CO_2 chemisorption efficiencies and that the temperature range for chemisorption was shifted to higher temperatures.

In a previous paper,[10] two different Li_4SiO_4 samples containing aluminum were prepared; $Li_{4.1}Al_{0.1}Si_{0.9}O_4$ and $Li_{3.7}Al_{0.1}SiO_4$. In these cases, it was observed that aluminum addition, into the lithium structural sites ($Li_{3.7}Al_{0.1}SiO_4$), improved the CO_2 capture at lower temperatures than Li_4SiO_4 and $Li_{4.1}Al_{0.1}Si_{0.9}O_4$. The authors argued that the vacancy doping seemed to be better than interstitial doping regarding the CO_2 chemisorption, facilitating O^{2-} hopping. In the present case, although the vacancy doping was produced in a different solid solution system ($Li_{4-x}(Si_{1-x}V_x)O_4$), it seemed not to increase the CO_2 chemisorption in any case.

In fact, these results clearly showed that vanadium addition, into the Li_4SiO_4 structure, hindered the CO_2 capture. Furthermore, vanadium inhibits, in some way, the lithium diffusion as the CO_2 capture was dramatically decreased. Although it has been probed that vanadium addition to the Li_4SiO_4 structure improves the ion conductivity importantly,[39] then, in this case, the diffusion processes must be highly inhibited by the vanadium secondary phases presented on the external shell of products.

The dynamic CO_2 chemisorptions presented in Figures 8 and 9 suggest that $Li_{4+x}(Si_{1-x}Al_x)O_4$ and $Li_{4-x}(Si_{1-x}V_x)O_4$ solid solutions may possess better reaction rates than Li_4SiO_4, as most of these samples presented slightly higher weight increments at $T \leq 400$ °C. It could be attributed to the structural defects produced in both solid solutions. Nevertheless, the largest CO_2 capture improvements were observed at $T > 500$ °C, once the Li_2CO_3 and $LiAlO_2$ or Li_3VO_4 external shell was produced, and different diffusion processes are required in order to continue the CO_2 capture. In a previous paper,[31] it was proposed that if the produced external shell is composed of Li_2CO_3 and other lithium phases, the CO_2 chemisorption process seems to be enhanced or decreased depending on the lithium diffusion coefficients of the formed lithium secondary phases. In these Li_4SiO_4 solid solutions, it is evident that Al and V addition modified in different manners the CO_2 chemisorption process. In the $Li_{4-x}(Si_{1-x}V_x)O_4$ cases, the CO_2 chemisorption is considerably diminished. In these samples, the product external shell is composed by Li_2CO_3, Li_2SiO_3, and Li_3VO_4 (see reaction 3). Additionally, it should be mentioned that Li_3VO_4 has a slower lithium diffusion coefficient than Li_2CO_3 and Li_2SiO_3.[48] Therefore, the presence of Li_3VO_4 on the external shell must reduce importantly the CO_2 chemisorption by decreasing the lithium diffusion; in comparison to the pure Li_4SiO_4 sample, which only contains Li_2CO_3 and Li_2SiO_3 on the external shell of products.

$$Li_{4-x}(Si_{1-x}V_x)O_4 + (1-x)CO_2 \rightarrow (1-x)Li_2CO_3 + (1-x)Li_2SiO_3 + xLi_3VO_4 \quad (3)$$

Conversely, the aluminum addition enhanced the CO_2 chemisorption on the Li_4SiO_4 solid solutions, and the most interesting behavior was produced at high temperatures, which is the process limited by the external shell. In this case, the CO_2 chemisorption, controlled by diffusion processes, can be divided in two temperature ranges: between 380 and 570 °C and between 600 and 770 °C. In this case, the lithium external shell is composed by Li_2CO_3, Li_2SiO_3, and $LiAlO_2$ (reaction 4). Therefore, the CO_2 chemisorption controlled by diffusion in $Li_{4+x}(Si_{1-x}Al_x)O_4$ samples is determined by different lithium secondary phases, depending on temperature. Between 380 and 570 °C, lithium diffusion must be promoted by Li_2CO_3 and Li_2SiO_3, as in the Li_4SiO_4 case. Nevertheless, at temperatures higher than 600 °C, a second diffusion process must be activated due to the $LiAlO_2$ presence, increasing the final CO_2 chemisorption. In fact, these results are in good agreement with the previous paper describing the diffusion effect produced by the presence of different lithium secondary phases,[31] and at the same time, the CO_2 chemisorption temperature ranges tend to be very similar than that observed on the Li_5AlO_4 sample.[16]

$$Li_{4+x}(Si_{1-x}Al_x)O_4 + (1+x)CO_2 \rightarrow (1+x)Li_2CO_3 + (1-x)Li_2SiO_3 + xLiAlO_2 \quad (4)$$

To further understand the CO_2 absorption on these ceramics, some extra experiments were performed. Figure 10 shows the isothermal graphs of the samples V20 and Al50 at different temperatures. These two samples were chosen because

dx.doi.org/10.1021/jp3006298 | J. Phys. Chem. A 2012, 116, 3163−3171

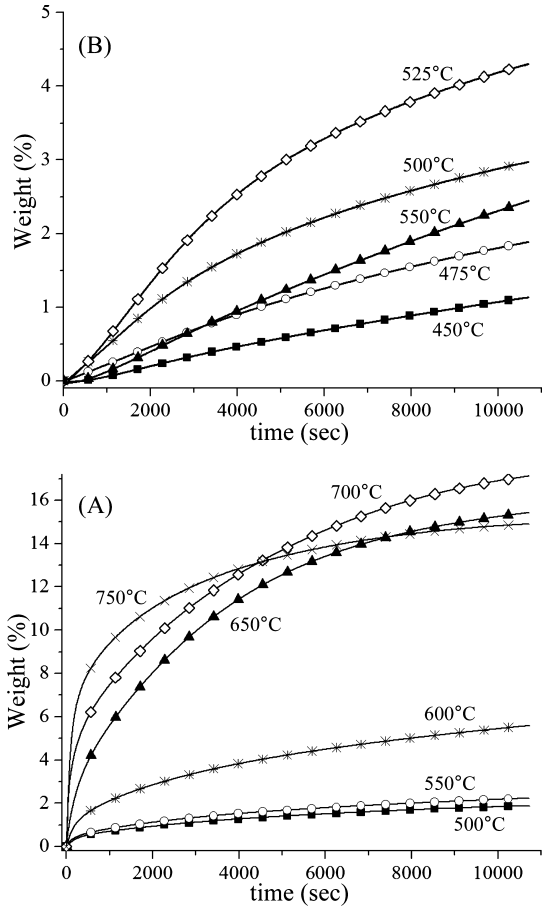

Figure 10. Isothermal analyses of the Al50 (A) and V20 (B) Li_4SiO_4 solid solutions at different temperatures in a flux of CO_2.

they contain the highest amount of vanadium and aluminum. The V20 isotherms were performed between 450 and 550 °C, according to the dynamic TG results. These isotherms presented a growing exponential behavior, where the CO_2 capture amounts varied from 1.1 wt % at 450 °C to 4.3 wt % at 525 °C. At the highest temperature (550 °C), the CO_2 capture was decreased to 2.9 wt %, as the absorption−desorption equilibrium was activated. On the contrary, the Al50 isotherms were performed between 500 and 750 °C because the CO_2 dynamic absorption was observed in this range. As expected, this sample presented a higher CO_2 absorption than the vanadium sample. At 500 and 550 °C, the Al50 sample only captured 1.8 and 2.7 wt %. This is in fact a weight percentage lower than those observed in the V20 sample at the same temperature range. However, when the temperature was increased between 650 and 750 °C, the highest CO_2 captures were observed. At 650 and 700 °C, the weight increments observed in these isothermal experiments were equal to 15.4 and 17.1 wt %, respectively. Finally, at 750 °C, the CO_2 desorption was activated, and the weight increment was slightly decreased to 14.9 wt %. Additionally, at this temperature, the Li_2CO_3 phase may have become liquid, affecting the CO_2 absorption−desorption equilibrium. All these results are in good agreement with the dynamic results presented previously in Figures 8 and 9.

4. CONCLUSIONS

$Li_{4+x}(Si_{1-x}Al_x)O_4$ and $Li_{4-x}(Si_{1-x}V_x)O_4$ solid solutions were prepared by solid state reaction. The analyses performed by XRD and MAS NMR strongly suggest that aluminum and vanadium are totally incorporated to the Li_4SiO_4 structure, occupying silicon atom sites.

Then, it was observed that vanadium and aluminum addition modified the CO_2 capture properties of Li_4SiO_4. In the vanadium solid solutions, the CO_2 capture was produced in the same temperature range as Li_4SiO_4, but the CO_2 capture capacity diminished when the vanadium content was incremented. On the contrary, the aluminum addition improved the CO_2 chemisorption on the solid solutions. The aluminum samples chemisorbed CO_2 in a wider temperature range than Li_4SiO_4. In fact, the most important CO_2 chemisorption was produced between 600 and 770 °C. This temperature shift is in good agreement with some Li_5AlO_4 reports. All these results were confirmed by a kinetic analysis.

According to these results, the CO_2 chemisorption process seems to be enhanced or decreased, not only depending on the structural modifications formed by doping but also in the lithium diffusion properties of the lithium secondary phases present in each case. Al and V addition modified importantly, but differently, the CO_2 chemisorption process. While on the $Li_{4-x}(Si_{1-x}V_x)O_4$ samples, the CO_2 chemisorption is considerably diminished, on the $Li_{4+x}(Si_{1-x}Al_x)O_4$ samples, the CO_2 capture was importantly improved. In these two solid solutions, the product external shell is composed of Li_2CO_3 and Li_2SiO_3 in both cases, and the unique difference is the presence of Li_3VO_4 or $LiAlO_2$. Then, it should be mentioned that Li_3VO_4 has a smaller lithium diffusion coefficient than Li_2CO_3, Li_2SiO_3, and $LiAlO_4$. Therefore, the presence of Li_3VO_4 on the external shell must reduce importantly the CO_2 chemisorption by decreasing the lithium diffusion; in comparison to the pure Li_4SiO_4 sample, which only contains Li_2CO_3 and Li_2SiO_3 on the external shell.

AUTHOR INFORMATION

Corresponding Author

*Phone: +52 (55) 5622 4627. Fax: +52 (55) 5616 1371. E-mail: pfeiffer@iim.unam.mx.

Notes

The authors declare no competing financial interest.

ACKNOWLEDGMENTS

This work was financially supported by the project SENER-CONACYT 150358. J.O.-L. thanks CONACYT for his scholarship. Finally, we thank E. Fregoso, G. Cedillo, and A. Tejeda for technical help.

REFERENCES

(1) Yun-Hang, H., Ed. *Advances in CO_2 Conversion and Utilization*; ACS Symposium Series 1056; American Chemical Society: Washington, DC, 2010.

(2) Choi, S.; Drese, J. H.; Jones, C. W. *ChemSusChem* **2009**, *2*, 796−854.

(3) Busch, A.; Alles, S.; Gensterblum, Y.; Prinz, D.; Dewhurst, D. N.; Raven, M. D.; Stanjek, H.; Krooss, B. M. *Int. J. Greenhouse Gas Control* **2008**, *2*, 297−308.

(4) Orr, F. M. Jr. *Energy Environ. Sci.* **2009**, *2*, 449−458.

(5) Nair, B. N.; Burwood, R. P.; Goh, V. J.; Nakagawa, K.; Yamaguchi, T. *Prog. Mater. Sci.* **2009**, *54*, 511−541.

(6) Mejía-Trejo, V. L.; Fregoso-Israel, E.; Pfeiffer, H. *Chem. Mater.* **2008**, *20*, 7171−7176.
(7) Pfeiffer, H.; Vazquez, C.; Lara, V. H.; Bosch, P. *Chem. Mater.* **2007**, *19*, 922−926.
(8) Pfeiffer, H.; Lima, E.; Bosch, P. *Chem. Mater.* **2006**, *18*, 2642−2647.
(9) Pfeiffer, H.; Bosch, P. *Chem. Mater.* **2005**, *17*, 1704−1710.
(10) Gauer, C.; Heschel, W. *J. Mater. Sci.* **2006**, *41*, 2405−2409.
(11) Veliz-Enriquez, M. Y.; Gonzalez, G.; Pfeiffer, H. *J. Solid State Chem.* **2007**, *180*, 2485−2492.
(12) Olivares-Marín, M.; Castro-Díaz, M.; Drage, T. C.; Maroto-Valer, M. M. *Sep. Purif. Technol.* **2010**, *73*, 415−420.
(13) Pacciani, R.; Torres, J.; Solsona, P.; Coe, C.; Quinn, R.; Hufton, J.; Golden, T.; Vega, L. F. *Environ. Sci. Technol.* **2011**, *45*, 7083−7088.
(14) Olivares-Marín, M.; Drage, T. C.; Maroto-Valer, M. M. *Int. J. Greenhouse Gas Control* **2010**, *4*, 623−629.
(15) Seggiani, M.; Puccini, M.; Vitolo, S. *Int. J. Greenhouse Gas Control* **2011**, *5*, 471−478.
(16) Ávalos-Rendón, T.; Casa-Madrid, J.; Pfeiffer, H. *J. Phys. Chem. A* **2009**, *113*, 6919−6923.
(17) Duan, Y.; Parlinski, K. *Phys. Rev. B* **2011**, *84*, 104113.
(18) Halabi, M. H.; de Croon, M. H. J.; van der Schaaf, J.; Cobden, P. D.; Schouten, J. C. *Chem. Eng. J.* **2011**, *168*, 872−882.
(19) Xiao, Q.; Tang, X.; Liu, Y.; Zhong, Y.; Zhu, W. *Chem. Eng. J.* **2011**, *174*, 231−235.
(20) Iwan, A.; Stephenson, H.; Ketchie, W. C.; Lapkin, A. A. *Chem. Eng. J.* **2009**, *146*, 249−258.
(21) Yin, X. S.; Zhang, Q. H.; Yu, J. G. *Inorg. Chem.* **2011**, *50*, 2844−2850.
(22) Rusten, H. K.; Ochoa-Fernández, E.; Lindborg, H.; Chen, D.; Jakobsen, H. A. *Ind. Eng. Chem. Res.* **2007**, *46*, 8729−8737.
(23) Yin, X. S.; Song, M.; Zhang, Q. H.; Yu, J. G. *Ind. Eng. Chem. Res.* **2010**, *49*, 6593−6598.
(24) Radfarnia, H. R.; Iliuta, M. C. *Ind. Eng. Chem. Res.* **2011**, *50*, 9295−9305.
(25) Yin, X. S.; Li, S. P.; Zhang, Q. H.; Yu, J. G. *J. Am. Ceram. Soc.* **2010**, *93*, 2837−2842.
(26) Xiao, Q.; Liu, Y.; Zhong, Y.; Zhu, W. *J. Mater. Chem.* **2011**, *21*, 3838−3842.
(27) Duan, Y. *J. Renewable Sustainable Energy* **2011**, *3*, 013102.
(28) Wang, K.; Guo, X.; Zhao, P.; Wang, F.; Zheng, C. *J. Hazard. Mater.* **2011**, *189*, 301−307.
(29) Mosqueda, H. A.; Vazquez, C.; Bosch, P.; Pfeiffer, H. *Chem. Mater.* **2006**, *18*, 2307−2310.
(30) Rodríguez-Mosqueda, R.; Pfeiffer, H. *J. Phys. Chem. A* **2010**, *114*, 4535−4541.
(31) Ortiz-Landeros, J.; Ávalos-Rendón, T. L.; Gómez-Yáñez, C.; Pfeiffer, H. *J. Therm. Anal. Calorim.* **2011**, DOI: 10.1007/s10973-011-2063-y.
(32) Robertson, A. D.; West, A. R.; Ritchie, A. G. *Solid State Ionics* **1997**, *104*, 1−11.
(33) Huggins, R. A. *Electrochim. Acta* **1977**, *22*, 773−781.
(34) Tilley, R. J. D. *Understanding Solids: the Science of Materials*; John Wiley & Sons, Ltd: New York, 2004.
(35) Saito, Y.; Ado, K.; Asai, T.; Kageyama, H.; Nakamura, O. *Solid State Ionics* **1991**, *47*, 149−154.
(36) Smith, R. I.; West, A. R. *J. Solid State Chem.* **1990**, *88*, 564−570.
(37) Khorassani, A.; West, A. R. *J. Solid State Chem.* **1984**, *53*, 369−375.
(38) Shannon, R. D.; Taylor, B. E.; English, A. D.; Berzins, T. *Electrochim. Acta* **1977**, *22*, 783−796.
(39) Jackowska, K.; West, A. R. *J. Mater. Sci.* **1983**, *18*, 2380−2384.
(40) Neudecker, B. J.; Weppner, W. *J. Electrochem. Soc.* **1996**, *143*, 2198−2203.
(41) Thangadurai, V.; Weppner, W. *Ionics* **2002**, *8*, 281−292.
(42) Weast, R. C.; Astle, M. J., Eds *CRC Handbook of Chemistry and Physics*, 63rd ed.; CRC: Boca Raton, FL, 1982.
(43) Rodriguez-Carvajal, J. *Computer Program FullProf*, version 3.51; Laboratoire Leon Brillouin CEA, CNRS: Grenoble, France, 1998.
(44) Caglioti, G.; Paoletti, A.; Ricci, F. P. *Nucl. Instrum. Methods* **1958**, *35*, 223−228.
(45) Stebbins, J. F.; Xu, Z.; Vollath, D. *Solid State Ionics* **1995**, *78*, L1−L8.
(46) Hennel, J. W.; Klinowski, J. *Fundamentals of Nuclear Magnetic Resonance*; Longman Scientific & Technical: New York, 1993.
(47) Xu, Z.; Stebbins, J. F. *Solid State Ionics* **1995**, *5*, 103−112.
(48) Mishra, K. M.; La, A. K.; Haque, F. Z. *Solid State Ionics* **2004**, *167*, 137−142.